Journal of Hydroscience and Hydraulic Engineering
Vol. 25, No.2 November, 2007, 23-35

MECHANISM OF DEOXYGENATION IN RESERVOIR METALIMNION

By

Kohji Michioku

Department of Civil Engineering, Kobe University, Rokkodai, Nada, Kobe, Japan

Hideyuki Kotani

East Japan Railway Co. Ltd., Yoyogi, Shibuya, Tokyo, Japan

Shigeta Sasaki

Nippon Steel Corporation Co. Ltd., Yoyogi, Shibuya, Tokyo, Japan

and

Yuhki Nishiguchi

CTI Engineering Co. Ltd., Ohtemae, Chuo, Osaka, Japan

SYNOPSIS

It was found in a eutrophic reservoir that the metalimnion became anoxic during the hot season while the hypolimnion became sufficiently aerated. The cause of metalimnion deoxygenation was investigated by means of field measurements. The field data suggests that dissolved oxygen in the metalimnion was more significantly consumed in the sidearm than in the main reservoir. The two mechanisms that may accelerate deoxygenation in the sidearm are discussed. The first one is the production and settling of organic matter in the sidearm, where greater algae blooming occurred than in the main reservoir, eventually leading to the long-term suspension of organic solids and the resultant oxygen consumption in the hypolimnion. Little oxygen is supplied there because the stable density stratification prevents the aerated hypolimnetic water from rising up. The second mechanism is the sediment oxygen demand that was most significant at a point where the metalimnetic water intersects the reservoir bed. Large amounts of nutrients, metals and other components were reduced from the sediment under such anaerobic conditions which increased the local water density and generated a horizontal intrusion of the anoxic hypolimnetic water into the main reservoir. At the same time this density current transported pollutants from the sidearm to the main reservoir.

INTRODUCTION

The reservoir is located in a narrow steep valley in Kobe, western Japan. A plane view of the reservoir is shown in Fig.1. The catchment area is 94.5 km^2, the water surface is 5.6 km long and the maximum water depth is

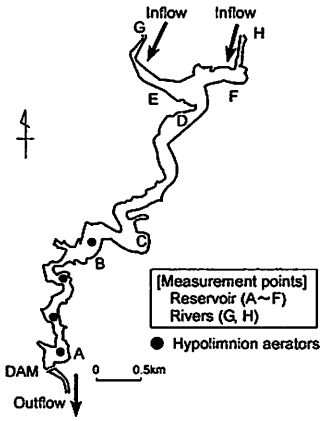

Fig.1 Locations of measurement points and hypolimnetic aerators

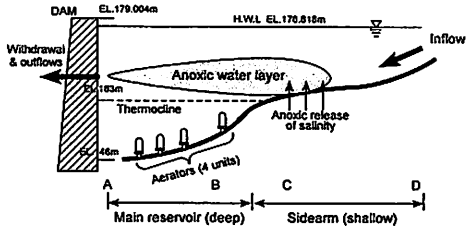

Fig.2 Schematic of reservoir cross section.

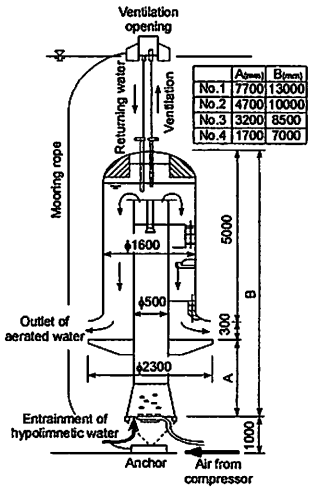

Fig.3 Aerator unit.

31 m. The total volume capacity is 11.6×10^6 m^3 and the annual river discharge is typically 7.15×10^7 m^3/year. Since the exchange rate of the impounded water, or the fraction of the annual discharge to the reservoir volume, ranges between 2.5 to 9.6, a stable thermal stratification develops during the hot season. Water is withdrawn from orifices located between 5.57 and 17.9 m below the high water level to supply drinking water to the Kobe City municipality. The reservoir has been subjected to deoxygenation and eutrophication and hypolimnetic aeration started in 1988. Four aerator units are installed as shown in Figs.1 and 2. The air discharge of each unit ranges between 350 and 1,500L/min. As is schematically shown in Fig.3, small air bubbles are generated at the base of the unit and the gas-liquid multi-phase flows entrains anoxic hypolimnetic water to the vertical cylinder. The water is aerated as it rises through the cylinder, and so the aerated water can be returned to the outlet. The residual air is ventilated to atmosphere without disturbing the impounded water. The system is designed so that aeration does not induce vertical mixing and the thermal stratification is kept stable.

Fig.4 shows a twenty-year period of variation of dissolved oxygen concentration observed at the main reservoir (Station A) and at the sidearm (Station C). Although the hypolimnion has been successfully aerated since 1988, the metalimnion has become particularly anoxic in the latest few years. Metalimnion deoxygenation causes more serious

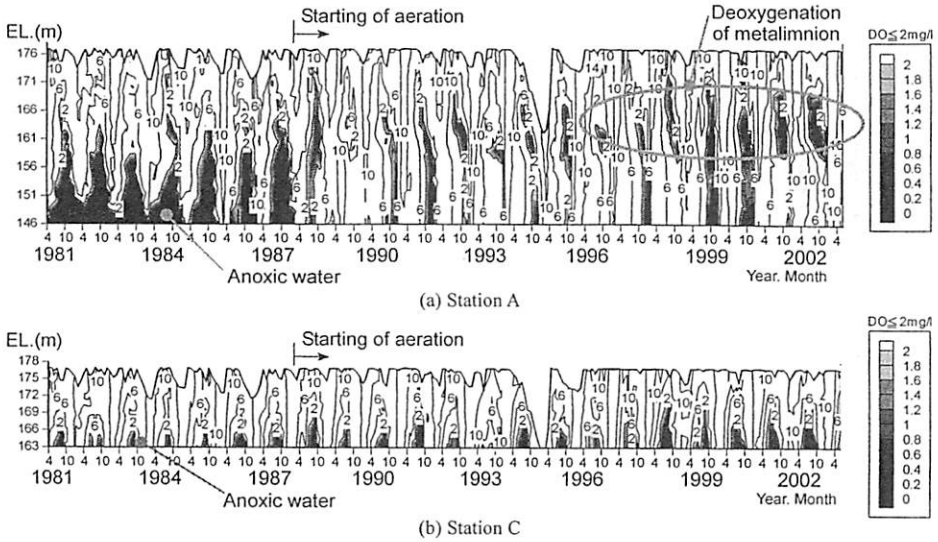

Fig.4 History of dissolved oxygen concentration. Unit is in mg/L.

problems than those associated with hypolimnion deoxygenation, because the metalimnion generally has a much greater volume than the hypolimnion; thus, a huge capacity aeration system is necessary for feeding oxygen there. In addition, the performance of the water purification plant located downstream of the reservoir has recently declined due to the withdrawal of the anoxic water from the metalimnion. Therefore, decisive measures must be adopted to solve the water quality problems. The focus of the present study is firstly to determine what causes the metalimnion deoxygenation and secondly to examine the countermeasures suitable for preventing metalimnion deoxygenation.

FIELD MEASUREMENTS

Field measurements were carried out from January 2004 to March 2006 to investigate how the metalimnion became anoxic. Monthly measurements of water quality were taken in the reservoir and at the inflows and outflow. The observed items were water temperature, turbidity, electric conductivity, dissolved oxygen, redox potential, chlorophyll-a, nitrogen, phosphorus, manganese, BOD, COD and pH. The water temperature, turbidity, electric conductivity, dissolved oxygen, redox potential, chlorophyll-a and pH were measured every 0.5m to 1.0m in the vertical direction by using a sensor probe. The nitrogen, phosphorus, manganese, BOD and COD were examined in a laboratory from water samples collected from three layers, i.e. 1m below the water surface, 1m above the reservoir bottom and a middle layer between the upper and lower layers, respectively. Additionally, in order to determine ignition loss, settled material was collected by using sediment traps every month from March 2004 to January 2005 at several points in the reservoir as listed in Table 1. In addition to the field data, water temperature, electric conductivity and dissolved oxygen before 2003 and meteorological and hydrological data were measured by the Water Works Bureau of Kobe City Authority. They were used in the data analysis.

Table 1 Measurement points of settled materials.

Station	Depth below water surface
A	5 m, 14 m, 20 m
B	5 m, 14 m
C	5 m, 10 m

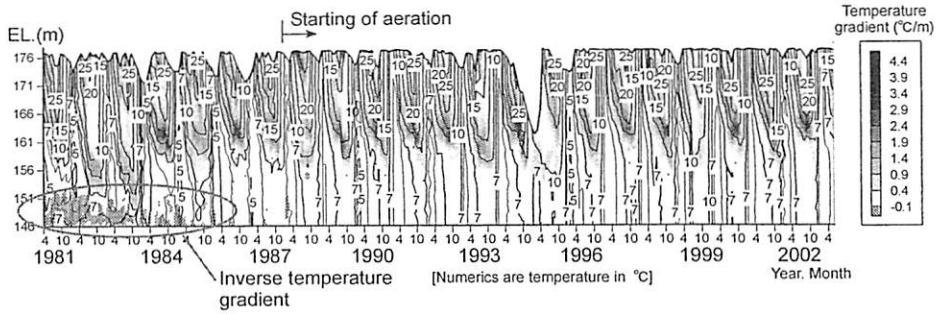

Fig.5 History of temperature structure observed at Station A during twenty years (Station A).

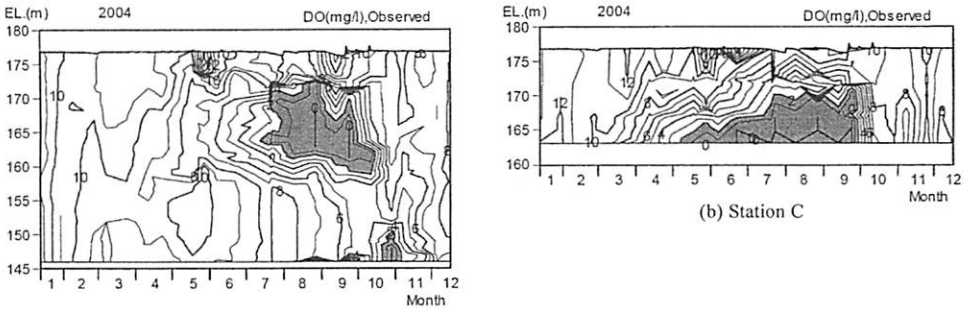

Fig.6 Comparison of DO contours at Stations A and C.

TEMPERATURE STRATIFICATION

A twenty year long history of temperature structure observed at Stations A is shown in Fig.5. The solid lines are isotherms of temperature and the gray patterns denote the vertical gradient of temperature. A stable thermal stratification develops during heating seasons. Before starting hypolimnetic aeration in 1987, the system was not completely overturned even in midwinter, and it remained meromictic. The other interesting feature is that inverse temperature stratification was found near the bottom. It is thought that this unstable temperature structure was gravitationally compensated by the high concentration of salinity there. After 1988, on the other hand, the reservoir was completely overturned in winter and the thermal structure remained holomictic. The formation mechanism of such a characteristic inverse temperature gradient is examined by means of a field measurement of thermosolutal density structure in reservoirs (3).

DISSOLVED OXYGEN

To show the seasonal behavior of dissolved oxygen, the DO concentrations observed at Stations A and C in 2004 are plotted in Fig.6. The concentration decreased to zero in May in the bottom layer at Station C. About a month later, the metalimnion at the main reservoir, "Station A", became anoxic. This finding revealed that DO was first consumed around Station C, and then the anoxic water mass spread downstream.

A correlation analysis was performed to estimate the traveling time of the anoxic water from Stations A to C. So-called the "template matching method" (4) was adopted for recognizing similar pattern of spatio-temporal structure of dissolved oxygen concentration between Station-A and C. As illustrated in Fig.7, the DO contour observed at

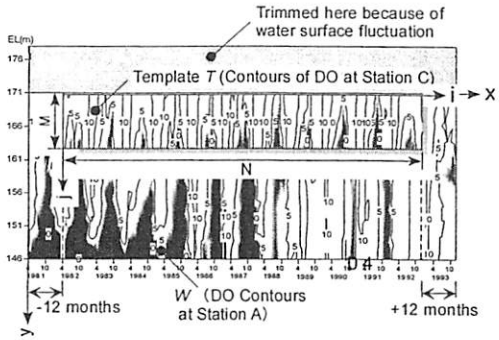

Fig.7 Pattern matching of DO contours between Stations A and C.

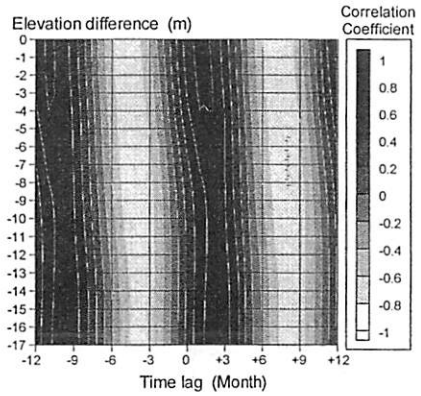

Fig.8 Spatiotemporal correlation coefficient between DO concentrations at Stations A and C.

Station C was used as a template and a spatio-temporal correlation coefficient with that observed at Station A was computed for varying elevation and time during 1996-2002 as follows:

$$R(x,y)=\frac{\sum_{i=1}^{N}\sum_{j=1}^{M}\left(W(x+i,y+j)-\overline{W}\right)\left(T(i,j)-\overline{T}\right)}{\sqrt{\sum_{i=1}^{N}\sum_{j=1}^{M}\left(W(x+i,y+j)-\overline{W}\right)^2}\sqrt{\sum_{i=1}^{N}\sum_{j=1}^{M}\left(T(i,j)-\overline{T}\right)^2}} \tag{1}$$

$$\overline{W}=\frac{1}{N}\frac{1}{M}\sum_{i=1}^{N}\sum_{j=1}^{M}W(x+i,y+j) \tag{2}$$

$$\overline{T}=\frac{1}{N}\frac{1}{M}\sum_{i=1}^{N}\sum_{j=1}^{M}T(i,j) \tag{3}$$

Here, $R(x, y)$ is the cross correlation coefficient of DO concentrations at Station A , $W(i, j)$, and that at Station C, $T(i, j)$. $\overline{W}$ and $\overline{T}$ are their averages. (x, y) are time and space coordinates directed as shown in Fig.7. (i, j) are indices of the data corresponding to (x, y), respectively, and (M, N) are the total numbers of the data. In the analysis, $T(i, j)$ was sampled from the range between the elevations of 163~171m during May in 1996 to June in 2002.

The results are shown in Fig.8, where darker color shows higher correlation. A high correlation can be observed in the time difference of one month and depth difference of 0 to -2m. This finding suggests that anoxic water produced in the bottom layer at Station C was almost horizontally transported downstream and arrived at Station A about one month later.

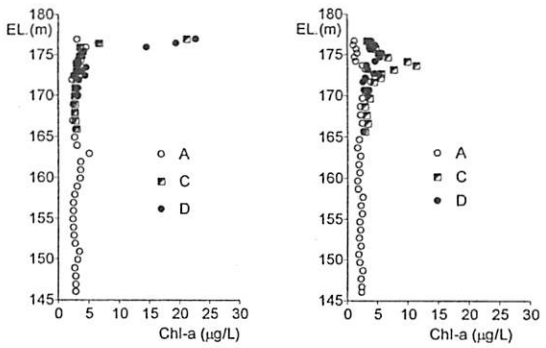

(a) 22 June (b) 23 July

Fig.9 Vertical profiles of chlorophyll-a concentration observed at Stations A, C and D in 2004.

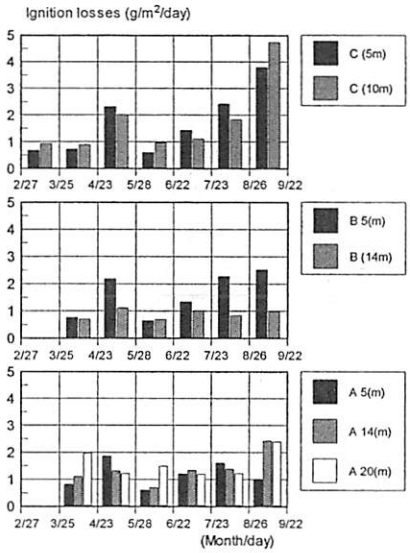

Fig.10 Ignition losses observed different layers at Stations A, B and C.

There might be two driving forces that transport the anoxic water. The first one is advection due to river through-flow. The mean flow velocity is estimated to be 4.6 km/month from the annual average discharge and cross section area of the epilimnion. Assuming the distance between Stations A and C is 2.5 kilometer, a rough estimation of the traveling time is 0.54 month. However, local flow that transports the anoxic water is considered to be slower than the averaged flow estimated in this way, because the motion is decelerated by the still hypolimnetic water. Upon considering this matter, the traveling time due to the through-flow was found to be approximately equivalent to the time lag obtained in the cross correlation analysis. It should be noted, however, that the traveling time estimation is based on a very rough idea of mean flow velocity and that the river through-flow is not the only mechanism of anoxic water transportation.

The second driving force is the gravity current generated by the density difference between the anoxic water and the ambient water (3). As will be discussed later, the anoxic water contains a high concentration of dissolved materials that eventually increases local salinity and fluid density. This may work as a gravitational driving force for horizontal intrusion.

Since both of the mechanisms contributed to the transportation of the anoxic water, the traveling time estimated

from the correlation analysis is an integrated result from the through-flow advection and the internal gravity current.

MECHANISM OF DEOXYGENATION AND POLLUTION IN METALIMNION

The question of why the metalimnion in the sidearm deoxygenated faster than in the main reservoir still must be solved. Here, we consider two possible mechanisms that may consume dissolved oxygen such as aerobic decomposition of suspended organic matter and sediment oxygen demand.

Oxygen consumption due to aerobic decomposition of suspended organic matter

Fig.9 shows the vertical profiles of chlorophyll-a observed at Stations A, C and D in June and July 2004. Higher products of photosynthesis were observed in the sidearm (Stations C and D) than in the main reservoir (Station A). This coincides with a general tendency that algae frequently bloom upstream in reservoirs, where nutrients fed from rivers are highly concentrated. The ignition losses which were observed at the Stations-A, B and C are plotted in Fig.10. IL at the Station C showed the most significant values. Particularly, settling amount of IL in a layer of 5 meters below the water surface and a settling of organic compounds were more significant at Stations B and C than at Station A, especially in summer. This explains how a higher concentration of organic matter is produced in the sidearm and suspended for a long duration in the metalimnion, which eventually brings about significant consumption of DO there. A large amount of suspended organic matters have often been observed around thermocline in other reservoirs, too (5).

Furthermore, a simple one-dimensional model is formulated in order to analytically describe organic matter balance and deoxygenation in a metalimnion. Assuming an equilibrium state in a vertical one-dimensional stratified system, a mass balance of chlorophyll-a is formulated as

$$\left(\underbrace{G_P}_{\text{Photosynthetic production}} - \underbrace{D_P}_{\text{Respiration, mortality and excretion}}\right) C_P - \underbrace{\frac{\partial}{\partial z}(w_S C_P)}_{\text{Settling}} + \underbrace{D\frac{\partial^2 C_P}{\partial z^2}}_{\text{Diffusion and resuspension due to turbulence}} = 0 \tag{4}$$

where C_P: concentration of chlorophyll-a in mg/L, G_P: photosynthetic growth rate of C_P and D_P: loss rate of C_P due to respiration, mortality and excretion. Both G_P and C_P are in 1/day. It is assumed that they are limited by nutrients, light and temperature as formulated by

$$G_P = \mu_{max}\beta_S f_{GP}(T) f(I) f(C_{IN}) f(C_{IP}) \tag{5}$$

$$D_P = k_{RP} f_{DP}(T) \tag{6}$$

where, μ_{max}: the maximum growth rate at 20℃ (=0.5/day), β_S: crowdedness coefficient of algae blooming, k_{RP}: coefficient of respiration, mortality and excretion (=0.05/day), I: the incoming irradiance, $f(I)$: limiting function of light, C_{IN} and C_{IP}: concentrations of nitrogen and phosphorus, respectively, $f_{GP}(T)$ and $f_{DP}(T)$: temperature limiting functions with respect to growth and loss of phytoplankton, T: water temperature in Celsius, $f(C_{IN})$ and $f(C_{IP})$: limiting functions of nitrogen and phosphorus. w_S(m/sec) is a settling velocity given by Stokes' law, assuming the mean diameter to be 10μm for the major species of mycrocistis (1).

As shown in Fig.11(a), a temperature profile is assumed to be a typical thermal structure during the heating season. A vertical profile of the turbulent diffusivity D in Fig.11(b) is given by

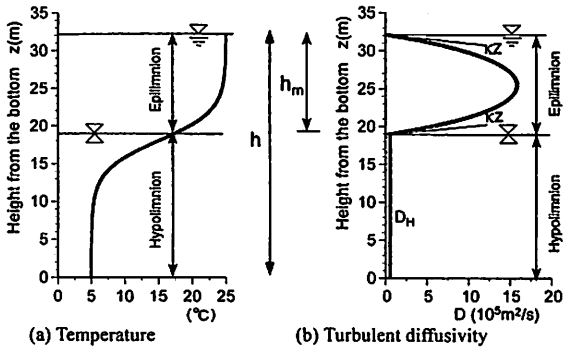

Fig.11 Assumed vertical profiles of temperature and turbulent diffusivity.

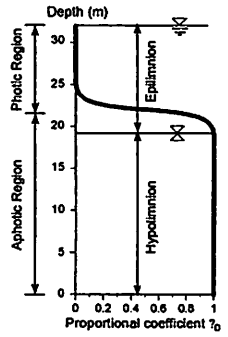

Fig.12 Assumed vertical profiles of proportional coefficient of D_T to C_P

$$D=\begin{cases} Au_*\kappa z\left(1-z/h_m\right)+D_H & \text{for } z\geq h-h_m \\ D_H & \text{otherwise} \end{cases} \tag{7}$$

where A is turbulent Schmidt number assumed to be A=1.0, κ=0.41 is Karman's constant, u_* is a friction velocity at the water surface, h_m is a surface mixed-layer thickness and D_H (=3x10^{-6}m^2/sec) is turbulent diffusivity in the hypolimnion determined by trial and error. Using a log law for a current driven by wind with a speed of U=0.5m/sec, the friction velocity u_* was given by Charnock's relationship (2).

Functional forms in Eqs.(4) through (6) are given by

(a) crowdedness coefficient (dimensionless): β_S

$$\beta_S=\exp[-\mu_S C_P] \tag{8}$$

where, μ_S is an empirical coefficient and assumed to be μ_S=0.0385 (L/mg).

(b) temperature limiting functions for growth and loss of algae: $f_{GP}(T), f_{DP}(T)$

$$f_{GP}(T)=\theta_{GP}^{(T-20)},\ f_{DP}(T)=\theta_{DP}^{(T-20)} \tag{9}$$

where, θ_{GP}(=1.25), θ_{DP}(=1.05).

(c) limiting function of light: $f(I)$

$$f(I)=\frac{I(z)}{I_{opt}}\exp\left[1-\frac{I(z)}{I_{opt}}\right] \tag{10}$$

where I_{opt} (W/m^2) is the optimum irradiance (=300) and the incoming irradiance (W/m^2) at the depth z, $I(z)$, is given by

$$I(z)=\left(1-\beta_L\right)Q'_S\exp[\eta(z-h)] \tag{11}$$

where β_L: absorption rate at the water surface (=0.45), Q_S' (w/m^2)(=750): solar energy flux or short wave radiation, h (=32m): the total water depth. η(m^{-1}) shows a light attenuation coefficient that is expressed as a function of C_P as

$$\eta=C_P+0.5 \tag{12}$$

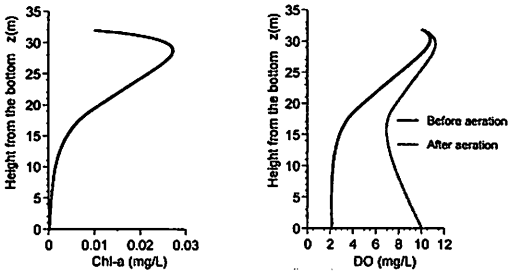

(a) Chlorophyll-a (b) DO concentration

Fig.13 Computed concentrations of chlorophyll-a and dissolved oxygen.

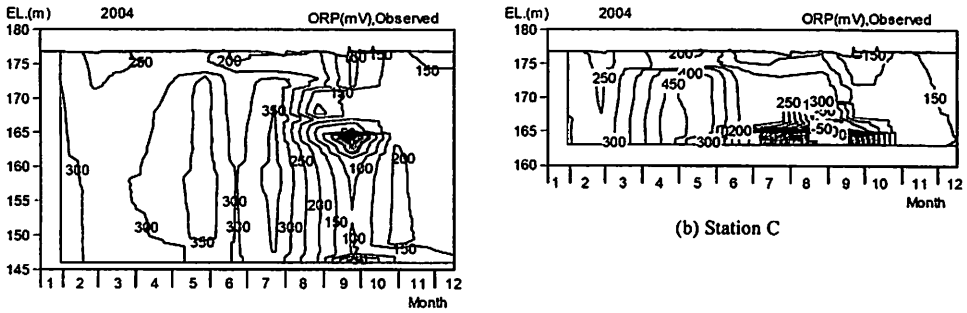

(a) Station A (b) Station C

Fig.14 Contours of redox potential, ORP, at Stations A and C.

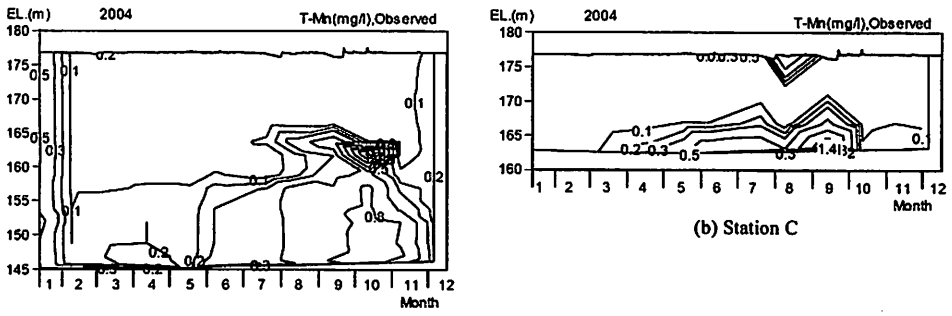

(a) Station A (b) Station C

Fig.15 Contours of total manganese, T-Mn, at Stations A and C.

(d) limiting functions of nutrients: $0 \le f(C_{IN}), f(C_{IP}) \le 1$

Although the Michaelis-Menten equation is generally used as a limiting function, they are assumed to be $f(C_{IN})=0.9$ and $f(C_{IP})=0.5$, respectively for analytical simplicity.

The balance of dissolved oxygen DO is then formulated by the following equation:

$$\underbrace{G_P \cdot C_P \cdot IC \cdot Y_{O,C} \cdot (1-K_P)}_{\text{Photosynthetic production}} - \underbrace{D_P \cdot C_P \cdot IC \cdot Y_{O,C}}_{\text{Respiration and mortality}} - \underbrace{k_{DT} \frac{DO}{K_{DT}+DO} f_{DT}(T) \cdot D_T}_{\text{Decomposition of organic matter}} + \underbrace{D \frac{\partial^2 DO}{\partial z^2}}_{\text{Turbulent diffusion}} = 0 \qquad (13)$$

Here, IC: ratio of carbon to chlorophyll-a (=44.4), $Y_{O:C}$: stoichiometric ratio of oxygen to carbon in photosynthesis

(=32.0/12.0), K_P: fraction of phytoplankton respiration relative to the total loss rate (=0.14/day), k_{DT}: decomposition rate of detritus (=0.3/day), K_{DT}(mg/L): half saturation constant for detritus decomposition (=1.1), $f_{DT}(T)$: temperature function as Eq.(9) and D_T(mg/l): concentration of detritus.

Since there is no information on D_T, D_T is assumed to be proportional to C_P as

$$D_T = \gamma_D C_P \tag{14}$$

Here, it is thought that most phytoplankton is alive in the photic region, while most of it is extinct in the aphotic region. Therefore, the coefficient γ_D is assumed to have a profile as shown in Fig. 12, where γ_D =0 in the photic region and γ_D =1 in aphotic region, respectively.

A set of solutions for C_P and *DO* are obtained by solving Eqs.(4) and (13) and their results are shown in Fig.13. Note that they are the approximate solutions obtained by giving typical values of the model parameters from literatures under assumption of a vertically one-dimensional system. In addition, the DO consumption from the bottom sediments is excluded in the analysis.

As shown in Fig.13(a), chlorophyll-a C_P increases in the photic layer and decreases in the aphotic layer, respectively. Since most of the suspended algae are trapped around the pycnocline, C_P decreases significantly in the hypolimnion. Dissolved oxygen *DO* is saturated in the epilimnion due photosynthesis and exchange across the air-water interface, while it significantly decreased in the hypolimnion. We assumed that the surface layer is saturated with oxygen, and *DO*=10mg/L is given as a boundary condition at the water surface instead of giving DO flux at the air-water interface. Equating *DO* with 10mg/L at the water-sediment interface for imitating the hypolimnetic aeration, a minimal of *DO* appeared around the thermocline. The findings suggest that one of the reasons for metalimnetic deoxygenation is that the oxygen consumption caused by decomposition of organic matters suspended around the pycnocline with high concentration.

Oxygen consumption by anoxic sediments

The second formation mechanism of the anoxic metalimnion is known as the sediment oxygen demand, SOD. Since a great amount of organic matter is accumulated on the sediment, it is thought that the redox potential of the sediment becomes critical around Station C. This phenomenon is confirmed from the contours of the redox potential, ORP, shown in Fig.14. It increases the desorption of nutrients and metals from the sediments. Fig.15, which shows the seasonal variations of total manganese, T-Mn, observed at the Stations A and C, indicates that manganese was first released from the bed under anaerobic conditions at Station C, and then a high concentration of T-Mn was detected at Station A a while later. Since there is no source of T-Mn around the metalimnion at Station A, the T-Mn observed there must be the component traveling from Station C. Under such anoxic conditions, other dissolved components such as ammonia, phosphate and ferrous iron might also be reduced, and they were also released from the anoxic sediment in addition to T-Mn. A salinity consisting of these highly concentrated dissolved compounds makes the anoxic water heavier than the ambient water.

Figs.14 and 15 indicate that the sidearm sediments produce anoxic and polluted water mass which was transported by a gravity undercurrent along the reservoir bed. The polluted undercurrent has higher density than the epilimnetic water due to salinity but is lighter than the hypolimnetic water because it is warmer than the hypolimnion. Therefore, the anoxic water horizontally intrudes into the metalimnion while being transported into the main reservoir. In this way, the anoxic metalimnion grows.

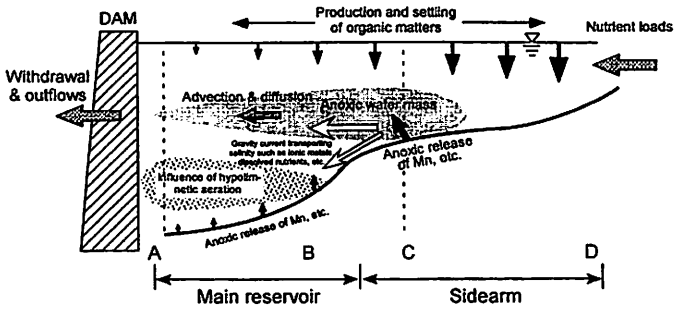

Fig.16 Schematic of metalimnion deoxygenation and related water quality phenomena.

CONCLUDING REMARKS

The mechanism of metalimnion deoxygenation is examined based on the field survey in a eutrophic reservoir. The findings of this study are schematically summarized in Fig.16. More organic matter is produced and settled in a shallow sidearm, "Station C", than in the main reservoir, "Station A". A high concentration of organic solids is suspended in the metalimnion and accumulated on the reservoir bed. A great deal of dissolved oxygen is consumed by the decomposition of the suspended and accumulated organic matter, which produce an anoxic water mass above the bed around Station C. Since thermal stratification prevents the aerated hypolimnetic water from reaching Station C, there is no oxygen supply to the bottom layer at Station C. Therefore, the anoxic layer grows more rapidly at Station C than at Station A. At the same time, many dissolved pollutants such as nutrients and metallic ions are released from the sediment through anoxic reduction, which increases the local density of the water and generates density currents running toward the main reservoir. Of course, the average river throughflow is another driving force for transporting the polluted metalimnetic water to the main reservoir. The traveling time from Station C to A is estimated to be about one month from a cross correlation analysis of water quality data.

The findings of the present study can provide some practical information for devising engineering countermeasures against metalimnetic water deoxygenation. Some techniques such as local aeration concentrated at the bottom layer of the sidearm, and minimizing photosynthesis at the surface layer of the reservoir upstream might be efficient ways of mitigating water quality problems.

REFERENCES

1. Arita,M. et al.: Environment in Hydrosphere, Tokyo Denkidaigaku Shuppankyoku, 1998 (in Japanese).
2. Deacon,E.L. and Webb,E.k.: Interchange of properties between sea and air, Ch.3, Small-scale interaction in the sea, ed.by M.B.Hill, Interscience, New York, pp.43-87, 1962.
3. Michioku, K. and Kanda, T.: Thermosolutal Stratification and Water Quality Behaviors in a Reservoir Hypolimnion before and after Micro-Bubble Aeration, Proc. 6th Intnl. Sympo. on Stratified Flows, CD-ROM, 2006.
4. Suematsu,R. and Yamada, H.: Image processing engineering, Corona Co.Ltd., 2000 (in Japanese).
5. Wetzel, R. G.: Limnology: Lake and River Ecosystems, Academic Pr, 1006P., 2001.

APPENDIX – NOTATION

The following symbols are used in this paper:

A = proportional coefficient in a formula giving turbulent diffusivity D;

C_P = concentration of chlorophyll-a;

C_{IN} = concentrations of nitrogen;

C_{IP} = concentrations of phosphorus;

D_P = loss rate of C_P due to respiration, mortality and excretion;

D_H = turbulent diffusivity in the hypolimnion;

D_T = concentration of detritus;

$f(I)$ = limiting function of light;

$f_{GP}(T)$ = temperature limiting functions respecting with growth of phytoplankton;

$f_{DP}(T)$: = temperature limiting functions respecting with loss of phytoplankton;

$f(C_{IN})$ = limiting functions of nitrogen;

$f(C_{IP})$ = limiting functions of phosphorus;

$f_{DT}(T)$ = temperature function as Eq.(8);

h = total water depth;

h_m =surface mixed-layer thickness;

(i, j) = indices of the data corresponding to (x, y), respectively;

I = incoming irradiance;

IC = ratio of carbon to chlorophyll-a (=44.4);

I_{opt} = the optimum irradiance (=300) at the depth z;

k_{RP} = coefficient of respiration, mortality and excretion;

k_{DT} = decomposition rate of detritus (=0.3/(24·60·60));

K_P = fraction of phytoplankton respiration relative to the total loss rate (=0.14/(24·60·60));

K_{DT} = half saturation constant for detritus decomposition (=1.1);

(M, N) = total numbers of the data in the correlation analysis;

Q_S' = solar energy flux or short wave radiation;

$R(x, y)$ = cross correlation coefficient between $W(i, j)$ and $T(i, j)$;

$T(i, j)$ = cross correlation coefficient of DO concentration at Station C;

u_* = friction velocity at the water surface;

U = wind with speed;

w_S = settling velocity for the major species of mycrocistis;

$W(i,j)$ = cross correlation coefficient of DO concentration at Station A;

$\overline{W}$ = average of $W(i,j)$;

(x, y) = time and space coordinates in Fig.7;

$Y_{O:C}$ = stoichiometric ratio of oxygen to carbon in photosynthesis (=32.0/12.0);

β_s = crowdedness coefficient of algae blooming;

β_L = absorption rate at the water surface (=0.45);

γ_D = proportional coefficient of D_T to C_P;

η = a light attenuation coefficient;

κ = Karman's constant (=0.41);

μ_{max} = maximum growth rate of C_P at 0℃;

μ_S = an empirical coefficient in a limiting function of crowdedness coefficient, Eq.(7), (μ_S=0.0385), and

θ_{GP}, θ_{DP} = empirical coefficients in a temperature limiting functions for growth and loss of algae.

(Received December 20, 2006 ; revised May 7, 2007)